https://doi.org/10.5194/essd-2026-143
Preprint. Discussion started: 9 March 2026

Open Access Earth System Science Data Discussions

SPAMS10: InSAR-derived soil motion parameters to model relative peat surface elevation changes

Yustisi Lumban-Gaol[1,2] and Ramon Hanssen[1]

[1]Department of Geoscience and Remote Sensing, Delft University of Technology, Delft, The Netherlands
[2]National Research and Innovation Agency, Jakarta, Indonesia

Correspondence: Yustisi Lumban-Gaol (y.a.lumbangaol@tudelft.nl)

Abstract. Peat subsidence poses a significant challenge to long-term land and environmental stability. Field monitoring with extensometers reveals variability in relative surface elevation changes, which are then modeled using simple parameterization for the motion of soils (SPAMS). To extend the spatial scale of monitoring, Interferometric Synthetic Aperture Radar (InSAR) time series are used. InSAR-derived SPAMS parameters provide meaningful displacement models that can describe peat subsidence and dynamics with a limited set of parameters. In this study, we publish the SPAMS10 dataset, which includes both physical and statistical parameters, along with additional contextual information at the parcel level. This dataset promotes data sharing among stakeholders, shifting products from InSAR-based relative elevation estimates to InSAR-derived displacement model parameters. These parameters enable detailed and reproducible analyses of peat subsidence. The dataset is available through the 4TU.ResearchData repository: https://doi.org/10.4121/dfbe9109-d058-4a64-a5b4-1cc9d9a5f836 (Lumban-Gaol et al., 2025) and is distributed under a Creative Commons Attribution 4.0 International (CC BY 4.0) license.

1 Introduction

Land subsidence, defined as the gradual downward displacement of the Earth's surface across extensive geographical regions relative to a designated reference level, represents a critical geophysical process with significant environmental implications. In peatland areas, anthropogenic activities such as lowering the water table for agricultural purposes and urban development have led to peat subsidence, a phenomenon often considered a "silent hazard" due to its slow progress but with severe environmental and socioeconomic consequences. This phenomenon contributes to numerous environmental challenges, including increased CO_2 emissions, flood risk, infrastructure damage, and reduced land productivity (Wösten et al., 1997; Page et al., 2011; Galloway and Burbey, 2011; Hooijer et al., 2012). Effective mitigation strategies require comprehensive monitoring systems to assess spatial and temporal impacts of the subsidence, supported by robust and scalable models of surface elevation changes.

Peat subsidence occurs mainly due to oxidation and compaction processes (Schothorst, 1977; Hoogland et al., 2012; Hooijer et al., 2012; van Asselen et al., 2018). Oxidation involves the decomposition of organic matter in aerated zones when exposed to oxygen, causing CO_2 emissions and volume reduction (Gambolati et al., 2005, 2006; van Huissteden et al., 2006; van Asselen et al., 2009). Compaction refers to the compression of soil under vertical effective stress from overburden weight and the reduced pore pressure resulting from oxidation (Stephens et al., 1984; van Asselen et al., 2009; Hooijer et al., 2012).

https://doi.org/10.5194/essd-2026-143
Preprint. Discussion started: 9 March 2026

Open Access Earth System Science Data Discussions

Efforts in monitoring peat subsidence have been continuously made using ground-based and remote sensing techniques, including leveling (Pleijter and van den Akker, 2007), extensometers (Van Asselen et al., 2020; Burbey, 2020), peat cameras (Evans et al., 2021), and interferometric synthetic aperture radar (InSAR) (Conroy et al., 2024). Modeling efforts incorporate these observations and peat subsidence processes, utilizing peat thickness and surface water levels to approximate the aerated zone thickness in order to estimate the subsidence rates (Hoogland et al., 2012), relating drainage depth and soil temperature to subsidence (Stephens et al., 1984; Zanello et al., 2011), and applying meteorological data to model soil surface motion (Conroy et al., 2023).

Despite these advances, the estimation of the elevation of peat soils from geodetic observations is still cumbersome. This is due to its high spatio-temporal variability, its sensitivity to land use, and the lack of well-identifiable benchmarks. Moreover, in the case of InSAR one also needs to resolve integer phase ambiguities and deal with loss-of-lock events, in which the connection between subsequent data acquisition is lost. To address this, we propose the SPAMS10 dataset. SPAMS10 refers to the descriptive displacement model: SPAMS (a Simple Parameterization for the Motion of Soils) and the number of parameters: ten. The dataset can be expressed as

$$\underline{\hat{x}} = \begin{bmatrix} \underline{\hat{x}}_{\mathrm{P}} \\ \underline{\hat{x}}_{\mathrm{E}} \\ \underline{\hat{x}}_{\mathrm{I}} \\ \tau \end{bmatrix} ; \ \mathrm{vech}(Q_{\hat{x}}) = \begin{bmatrix} \sigma^2_{\hat{x}_{\mathrm{P}}} \\ \sigma_{\hat{x}_{\mathrm{P}}\hat{x}_{\mathrm{E}}} \\ \sigma_{\hat{x}_{\mathrm{P}}\hat{x}_{\mathrm{I}}} \\ \sigma^2_{\hat{x}_{\mathrm{E}}} \\ \sigma_{\hat{x}_{\mathrm{E}}\hat{x}_{\mathrm{I}}} \\ \sigma^2_{\hat{x}_{\mathrm{I}}} \end{bmatrix}, \tag{1}$$

which includes the four SPAMS soil motion parameters $\underline{\hat{x}}$: the scaling factor of precipitation $\underline{\hat{x}}_{\mathrm{P}}$, the scaling factor for evapotranspiration $\underline{\hat{x}}_{\mathrm{E}}$, the irreversible subsidence rate $\underline{\hat{x}}_{\mathrm{I}}$ in mm/day, and the integration time τ in days. The underline indicates the stochastic nature of the estimate. The integration time τ is estimated and has a rather constant value, with a mean of 69 days and a standard deviation of two days. For convenience, we treat this parameter as deterministic and do not include it in the stochastic model. Focusing only on the first three parameters, we use the six statistical variance and covariance terms $\mathrm{vech}(Q_{\hat{x}})$ of the first three parameters for each parcel.

The parameters $\hat{x}$ and the half-vectorized covariance matrix, $\mathrm{vech}(Q_{\hat{x}})$, define the SPAMS10 dataset. These components serve as inputs for the SPAMS model (Conroy et al., 2023) to simulate relative elevation changes, enabling the modeling of both reversible and irreversible surface elevation changes and the quantification of the associated uncertainties. They also enable the forecasting of past and future subsidence under the assumption that conditions such as soil stratigraphy, groundwater management, and land use remain constant over time.

We focus on a region particularly vulnerable due to extensive agricultural use and underlying soft soils. The dataset covers 1,542 agricultural parcels over approximately 147 km^2, see Figure 1. Realizations of relative surface elevation based on SPAMS10 estimates of irreversible annual subsidence rates are critical for purposes such as assessing gas emissions and flood risk. The SPAMS10 parameters are intended as a first approximation and will be updated as the displacement model and geophysical understanding of the study area evolve.

https://doi.org/10.5194/essd-2026-143
Preprint. Discussion started: 9 March 2026

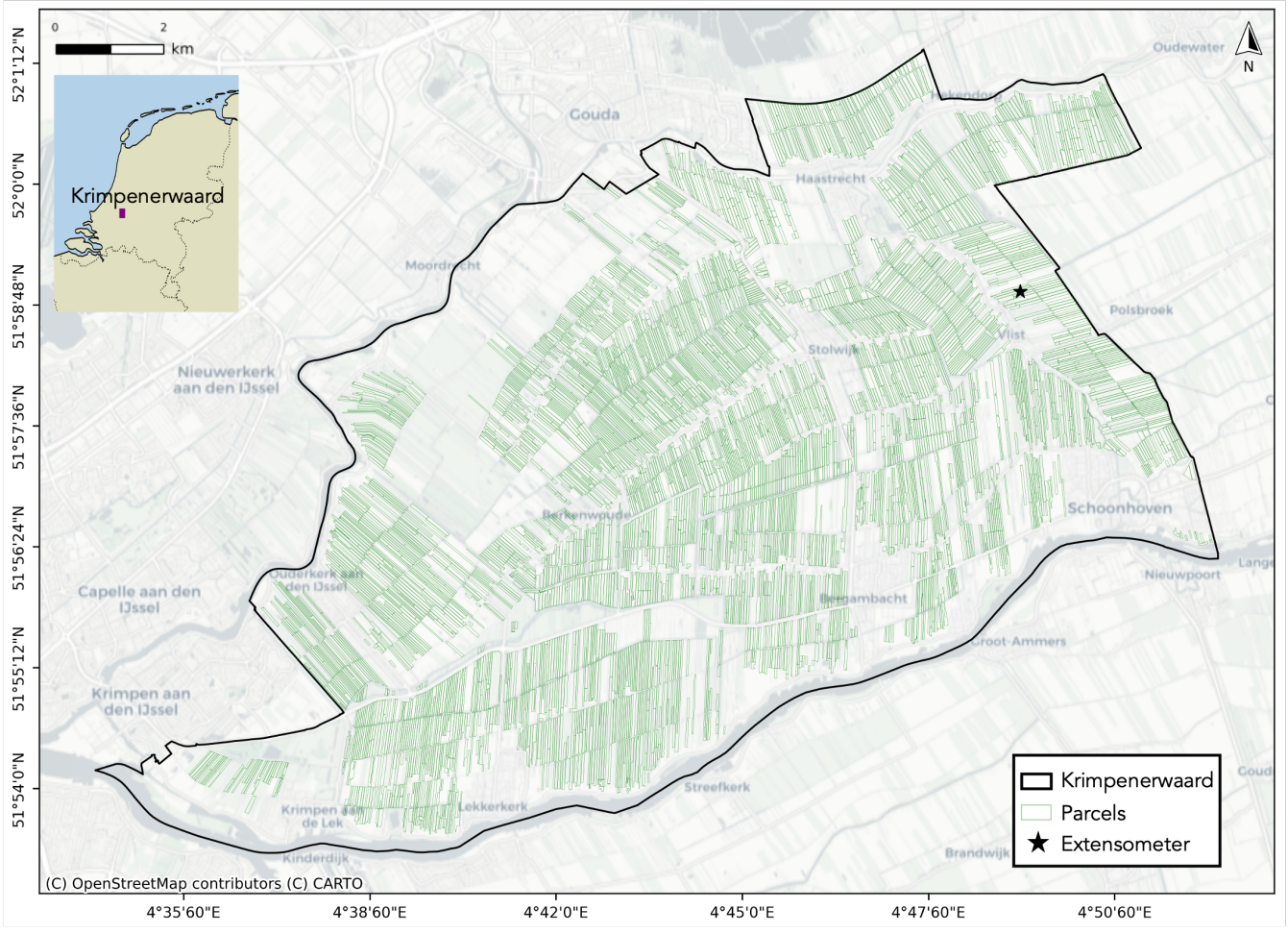

Figure 1. Krimpenerwaard study area overlayed with parcel polygons having the estimated SPAMS10 parameters. The extensometer site is used for validation purpose.

2 Methods

The SPAMS10 dataset is derived from a multi-stage methodology that uses InSAR observations with SPAMS as the displacement model. This study uses Sentinel-1A/B satellite acquisitions with the interferometric wide swath mode and a single VV polarization. Four satellite tracks, two ascending (088 and 161) and two descending (37 and 110), illuminate the area of interest, which is the Krimpenerwaard region in the Netherlands. We use data from 2015 to 2022, with a total number of acquisition of 370, 379, 383, and 386, respectively. All single look complex (SLC) images are preprocessed using Doris (Kampes and Usai, 1999; Kampes et al., 2004; Arikan et al., 2008) for coregistration.

The resulting coregistered SLC stack undergoes two separate analyses, for distributed scatterers (DS) and for point scatterers (PS). During DS analysis, the SLC images are multilooked over a window of Ω pixels within the known parcel geometry to

https://doi.org/10.5194/essd-2026-143
Preprint. Discussion started: 9 March 2026

estimate the full complex coherence matrix $\hat{\Gamma}$. This matrix describes the degree of similarity between pairs of SAR images for all possible combinations of N SAR acquisitions, per parcel. It is used as a metric for the precision of the interferometric phase. The matrix is defined as

$$\hat{\Gamma} = \begin{bmatrix} \hat{\gamma}_{11} & \hat{\gamma}_{12} & \cdots & \hat{\gamma}_{1N} \\ \hat{\gamma}_{21} & \hat{\gamma}_{22} & \cdots & \hat{\gamma}_{2N} \\ \vdots & \vdots & \ddots & \vdots \\ \hat{\gamma}_{N1} & \hat{\gamma}_{N2} & \cdots & \hat{\gamma}_{NN} \end{bmatrix}, \tag{2}$$

where $\hat{\gamma}$ is the complex coherence estimator, expressed as (Hanssen, 2001)

$$\hat{\gamma}_{ij} = \frac{\sum_{n\in\Omega} y_i^{(n)} y_j^{*(n)}}{\sqrt{\left(\sum_{n\in\Omega} \left|y_i^{(n)}\right|^2\right)\left(\sum_{n\in\Omega} \left|y_j^{(n)}\right|^2\right)}}, \tag{3}$$

where $y_i^{(n)}$ and $y_j^{(n)}$ are the complex values of pixel n in image i and j. Pixel n is within the window Ω, and $(\cdot)^*$ denotes the complex conjugate. Based on the estimate of the full complex coherence matrix we estimate a single set of DS phases, equivalent to those obtained from interferometric combinations with one reference image. We refer to this as the equivalent single mother phase $\hat{\phi}_{\mathrm{ESM}}$. By applying the eigendecomposition-based maximum likelihood estimator of interferometric phase (Ansari et al., 2018) to the full coherence matrix, the complete set of interferometric combinations is reduced to a single set of phases. Assuming unbiased estimation, the phase variance follows the Cramer-Rao bound $\sigma^2_{\hat{\phi}_{ij,\mathrm{CRB}}}$, which is expressed as (Hanssen, 2001)

$$\sigma^2_{\hat{\phi}_{ij,\mathrm{CRB}}} = \frac{1-|\gamma_{ij}|^2}{2L|\gamma_{ij}|^2}, \tag{4}$$

where L is the effective number of looks, which is the ratio between the number of pixels Ω within an estimate window and the oversampling ratio (Hanssen, 2001). Based on these procedures, we obtain a phase time series per parcel, together with its estimation quality, denoted as

$$\hat{\phi}_{\mathrm{ESM}} = \begin{bmatrix} \hat{\phi}_1 & \hat{\phi}_2 & \cdots & \hat{\phi}_N \end{bmatrix}^T, \quad Q_{\phi_{\mathrm{ESM}}} = \begin{bmatrix} \sigma^2_{11} & \sigma^2_{12} & \cdots & \sigma^2_{1N} \\ \sigma^2_{21} & \sigma^2_{22} & \cdots & \sigma^2_{2N} \\ \vdots & \vdots & \ddots & \vdots \\ \sigma^2_{N1} & \sigma^2_{N2} & \cdots & \sigma^2_{NN} \end{bmatrix}. \tag{5}$$

From the same coregistered SLC stack, the atmospheric phase screen (APS) is estimated using a PS network, following the DePSI framework (Van Leijen, 2014). To perform APS filtering, we first need to disentangle the atmospheric signal from other phase contributions, such as displacement signals. The atmospheric signals are assumed to be correlated in space but uncorrelated in time (Ferretti et al., 2001), while the displacement signals are assumed to be correlated in time with limited spatial correlation. The noise is considered to be uncorrelated in both space and time. Using these spatio-temporal characteristics, the

https://doi.org/10.5194/essd-2026-143
Preprint. Discussion started: 9 March 2026

Open Access Earth System Science Data Discussions

atmospheric signal delay at the selected PS is isolated, and the APS for the full interferogram scenes is estimated using Kriging (Krige, 1951). We combine the DS per parcel with the available PS for atmospheric filtering. Each parcel is treated as a virtual PS, with the parcel centroid as the virtual point.

Up to this point, we have obtained a set of modulo-2π phases measured along the radar line of sight. These are associated with integer phase ambiguities that must be resolved to derive a proper time series representing relative elevation changes. This process typically relies on assumptions and the applied functional models. In peatlands, we assume that surface elevation changes are driven by environmental (meteorological) conditions. Thus, we use the SPAMS (Simple Parameterization for the Motion of Soils) model developed by Conroy et al. (2023) as the functional model used to estimate both the displacement model parameters and the integer phase ambiguities. The SPAMS model is expressed as

$$h_{\mathrm{SPAMS}}(t) = \underbrace{\sum_{k=t-\tau}^{t} \left(x_{\mathrm{P}} P(k) - x_{\mathrm{E}} E(k)\right)}_{\text{reversible } R(t)} + \underbrace{\sum_{s=1}^{t} x_{\mathrm{I}} \cdot f(s)}_{\text{irreversible } I(t)}, \tag{6}$$

$$\text{where } f(s) = \begin{cases} 0, & \text{for } R(t) > 0, \\ 1, & \text{for } R(t) \leq 0. \end{cases}$$

The modeled elevation is projected onto the line of sight towards the radar and converted to radians, comparable to the InSAR observations, with

$$W\left\{\phi_{\mathrm{SPAMS}}(t)\right\} = W\left\{\frac{-4\pi \cos\theta_{\mathrm{inc}}}{\lambda} \cdot h_{\mathrm{SPAMS}}(t)\right\}, \tag{7}$$

where θ_{inc} is the incidence angle, λ is the wavelength, and $W\{\cdot\}$ is the wrapping operator (Hanssen, 2001).

The SPAMS model estimates the relative[1] surface elevation h at time t using precipitation (P) and evapotranspiration (E) data from nearby meteorological stations. It incorporates four parameters to be estimated: the scaling factor for precipitation x_{P}, the scaling factor for evapotranspiration x_{E}, the irreversible subsidence rate x_{I} in mm/day, and the inertia or integration time τ in days. The model describes surface motion as consisting of a reversible component $R(t)$ and an irreversible component $I(t)$, where the latter is only active during a precipitation deficit ($R(t) \leq 0$). These parameters are estimated with an iterative workflow using the observed modulo-2π InSAR phases (Conroy and Hanssen, 2025). Within this framework, the emphasis shifts from resolving phase ambiguities to parameterizing the displacement model and estimating its parameters.

The initial estimation is performed on the parcel level. Due to irrecoverable temporal decorrelation, e.g., ploughing events, we have gaps in the time series data. We split the data into several coherent segments and introduce an unknown vertical displacement parameter, Δz, between segments, specific to each parcel and observation epoch. The segmentation of the observed phases is performed based on the coherence between subsequent acquisitions (here referred to as 'daisy chain'), $|\hat{\gamma}_{\mathrm{DC}}|$, and the number of consecutive coherent epochs. The daisy chain coherence is equivalent to the first off-diagonal of the full coherence matrix $|\hat{\Gamma}|$ of each parcel. In our case, a minimum of two consecutive epochs with $|\hat{\gamma}_{\mathrm{DC}}| > 0.19$ is used as a threshold to distin-

[1] In the forward model, the elevation is relative to the arbitrary elevation of the surface during the first observation epoch.

https://doi.org/10.5194/essd-2026-143
Preprint. Discussion started: 9 March 2026

Open Access Earth System Science Data Discussions

guish segments, based on experience. To account for the unknown shifts between segments, we take the differences between subsequent phases. This forms a set of disconnected daisy chain segments, where each segment starts at zero.

Using an initial set of parameters, the optimal model parameters estimation is performed by iteratively searching the parameter space $\hat{x}$ while maximizing the temporal coherence estimates $\hat{\gamma}_{\text{temp}}$ between the modeled and observed daisy chain phases in all coherent segments, denoted by

$$\hat{\gamma}_{\text{temp}} = \frac{1}{T}\left|\sum_{t=1}^{T}\exp\{j[\Delta\phi_{\text{IP}}(t) - \Delta\hat{\phi}_{\text{SPAMS}}(t)]\}\right|, \tag{8}$$

where $\Delta\phi_{\text{IP}} \in [-\pi, +\pi) \subset \mathbb{R}$ is the daisy chain modulo-2π interferometric phase observation, $\Delta\phi_{\text{SPAMS}} \in \mathbb{R}$ is the daisy chain phase model, t is epoch, and T is the number of epochs in all coherent segments.

Within the initial estimation, we obtain the optimal set of model parameters, which implicitly yields the corresponding integer ambiguities. The absolute observed phases are then computed per segment, i.e., the time series remain disconnected across segments. To connect them, we need to shift each segment according to the unknown offsets, which are estimated as

$$\hat{\phi}_{\Delta\hat{z},s} = \langle\hat{\phi}_{\text{IP}_s} - \hat{\phi}_{\text{SPAMS}_s}\rangle. \tag{9}$$

where $\hat{\phi}_{\Delta\hat{z},s}$ is the unknown offset at segment s, $\hat{\phi}_{\text{IP}_s} \in \mathbb{R}$ and $\hat{\phi}_{\text{SPAMS}_s} \in \mathbb{R}$ are the estimated absolute observed and modeled phases at segment s, respectively, and $\langle\cdot\rangle$ denotes the averaging operator. The segment offset estimation results in a set of continuous estimates for the InSAR epochs from all satellite tracks. For a single parcel, this estimate is denoted as

$$\hat{y}_{\text{IP}} = \frac{-\lambda}{4\pi}\begin{bmatrix} \hat{\phi}^{\text{I}}_{\text{IP},t\in T}/\cos\theta^{\text{I}}_{\text{inc}} \\ \hat{\phi}^{\text{II}}_{\text{IP},t\in T}/\cos\theta^{\text{II}}_{\text{inc}} \\ \hat{\phi}^{\text{III}}_{\text{IP},t\in T}/\cos\theta^{\text{III}}_{\text{inc}} \\ \hat{\phi}^{\text{IV}}_{\text{IP},t\in T}/\cos\theta^{\text{IV}}_{\text{inc}} \\ \vdots \end{bmatrix}, \tag{10}$$

where $\hat{y}_{\text{IP}}$ is the vector of InSAR-based relative elevation estimates, $\hat{\phi}_{\text{IP}}$ are the shifted absolute observed phases, t is the epoch, T is the set of epochs in all coherent segments in all tracks, and the superscript indicates the satellite track number, where I, II, III, and IV represent track a088, d037, d110, and a161, respectively.

Following per-parcel estimation, a group estimation is performed to re-estimate the model parameters, especially the irreversible $\hat{x}_I$, as well as the ambiguities and segment shifts. We group parcels by soil type and water table zone, and include only grassland parcels. The contextual grouping reduces the number of segments, thereby aiming to reduce segment shift noise. The group is formed if there are at least 15 and no more than 50 parcels.

The group estimation framework is similar to the initial per-parcel estimation. We use the average parameter values of parcels having $\hat{\gamma}_{\text{temp}} \geq 0.15$ within a group as initial parameters when tuning the model parameters at the group level. The parameters are estimated by minimizing the root mean squared error (RMSE) between the model and the median group elevation based on the initial estimates.

https://doi.org/10.5194/essd-2026-143
Preprint. Discussion started: 9 March 2026

Open Access Earth System Science Data Discussions

Once an optimal set of parameters is found, the model elevation at parcel level is estimated using the parameters $\hat{x}_P$ and $\hat{x}_E$ from the initial estimation, as well as the parameter $\hat{x}_I$ and τ from the group estimation. Following the formulation of the SPAMS model in equation (6), the linearized matrix form is

$$\hat{y}_{\text{SPAMS}} = B\hat{x}, \tag{11}$$

where

$$B = \begin{bmatrix} \sum_{k=t_1-\tau}^{t_1} P(k) & -\sum_{k=t_1-\tau}^{t_1} E(k) & \sum_{s=1}^{t_1} \hat{f}(s) \\ \vdots & \vdots & \vdots \\ \sum_{k=t_n-\tau}^{t_n} P(k) & -\sum_{k=t_n-\tau}^{t_n} E(k) & \sum_{s=1}^{t_n} \hat{f}(s) \end{bmatrix}, \quad \hat{x} = \begin{bmatrix} \hat{x}_{\text{P}} \\ \hat{x}_{\text{E}} \\ \hat{x}_{\text{I}} \end{bmatrix} \tag{12}$$

where n denotes daily SPAMS model epochs. Using only the model elevation at InSAR coherent epochs, the segment shifts are re-estimated following equation (9), producing an updated InSAR-based relative elevation estimate.

Finally, a final per-parcel estimation is performed by minimizing the RMSE between the InSAR-based relative elevation estimates $\hat{y}_{\text{IP}}$ and the model $\hat{y}_{\text{SPAMS}}$. The final output parameters become the model parameter estimates $\underline{\hat{x}}$ in the SPAMS10 dataset, as in equation (1).

The uncertainty of the model parameters is then propagated as

$$Q_{\hat{x}} = (B^T Q_y^{-1} B)^{-1}, \tag{13}$$

where Q_y is the variance matrix of the contextual group phase observations projected onto the vertical following the satellite tracks. The variance σ^2 of an epoch in a particular satellite track can be denoted as

$$\sigma_y^2 = (\sigma_{\phi_{\text{group}}} \cdot \frac{\lambda}{4\pi \cos\theta_{\text{inc}}})^2, \tag{14}$$

where $\sigma_{\phi_{\text{group}}}$ is the standard deviation of the estimated absolute observed phases within a contextual group. The output $Q_{\hat{x}}$ is a symmetrical matrix 3×3 where the diagonal values are the variance of each estimated parameter and the off-diagonal values are the covariance between parameters. Since the upper and lower diagonal have the same value, we denote it as the half vectorization $\text{vech}(Q_{\hat{x}})$ as in equation (1).

3 Results and Technical Validation

Figures 2a-c show the spatial distribution of the InSAR-derived soil motion parameters used to model relative surface elevation changes at the parcel level. Statistically, the median precipitation scaling factor x_{P} is $\sim 7.29 \times 10^{-2}$, while the median evapotranspiration scaling factor x_{E} is $\sim 13.40 \times 10^{-2}$. The median irreversible rate x_{I} across the study area is $\sim -2.77 \times 10^{-2}$mm/day. The figure also shows that some parcels still lack parameter estimates. These parcels are excluded either due to their crop type or because there are too few parcels to form a contextual group. Further methodological development is required to enable analysis in agricultural land with more complex surface dynamics.

https://doi.org/10.5194/essd-2026-143
Preprint. Discussion started: 9 March 2026

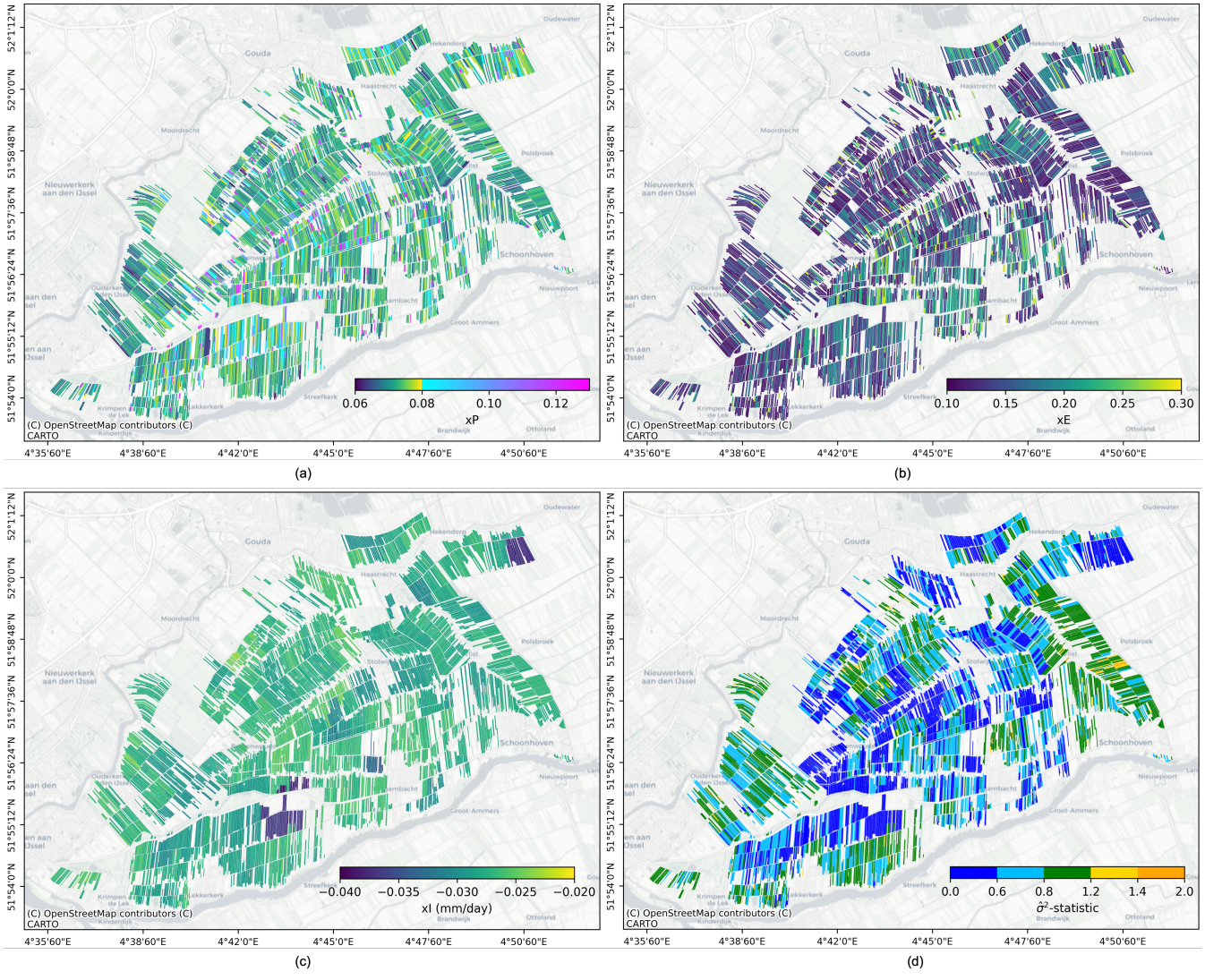

Figure 2. Spatial distributions of the scaling factor of precipitation $\hat{x}_{\mathrm{P}}$ (a), the scaling factor of evapotranspiration $\hat{x}_{\mathrm{E}}$ (b), the subsidence rate $\hat{x}_{\mathrm{I}}$ in mm/day (c), and $\hat{\sigma}^2$ test statistic (d).

The quality is measured based on the $\hat{\sigma}^2$ test statistic to evaluate the functional and stochastic model in relation to the observations. This evaluation is computed based on the sum of squared residuals, weighted by the inverse of the variance-
170 covariance matrix of the observations, between InSAR displacement estimates projected onto the vertical and the SPAMS elevation model, normalized by the degrees of freedom for each parcel, which is expressed as (Teunissen, 2024)

$$\underline{\hat{\sigma}}^2 = \frac{\underline{\hat{e}}^T Q_y^{-1} \underline{\hat{e}}}{m-n}, \tag{15}$$

https://doi.org/10.5194/essd-2026-143
Preprint. Discussion started: 9 March 2026

Open Access Earth System Science Data Discussions

where $\hat{\underline{e}}$ is the vector of residuals between the InSAR-based relative elevation estimates and the SPAMS model, Q_y is the variance-covariance matrix of the observables where the values are described as in equation (14), m is total number of observations, and n is total number of estimated parameters. The $\hat{\sigma}^2$ test statistic values are non-negative numbers, typically ranging from 0.1 to 1.9 for the area of interest with a distribution depicted in Figure 2d. Values close to one suggest sufficient alignment between the model and the observations. Values larger than one indicate model imperfections or an overly optimistic stochastic model. On the contrary, values significantly smaller than one indicate an overly pessimistic stochastic model (or over-parameterized functional model).

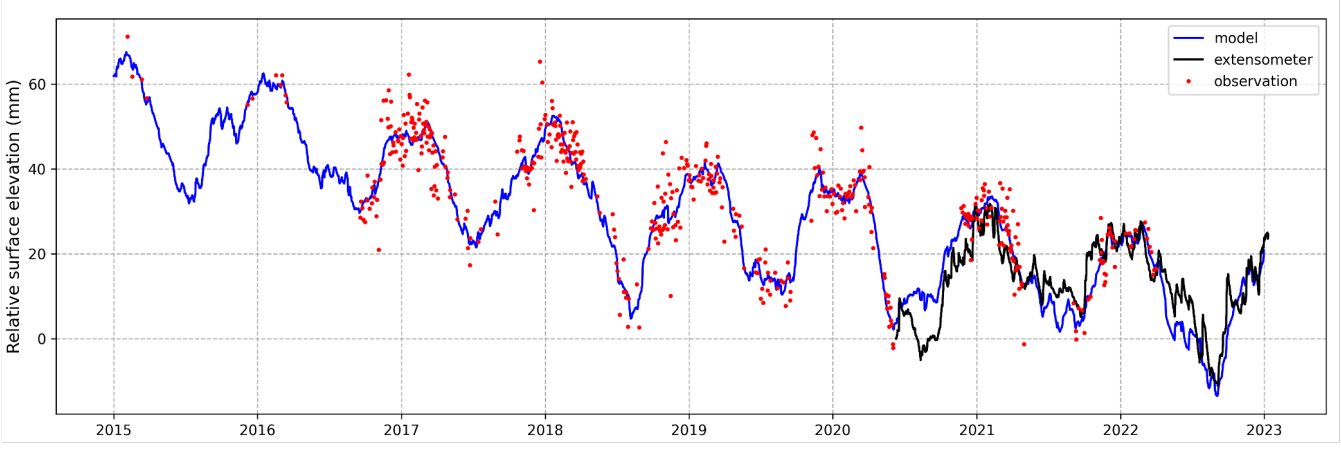

Figure 3. Comparison of relative surface elevation changes from extensometer data (black line), InSAR-based relative elevation estimates (red dots), and the SPAMS model (blue line) showing similar agreement levels. The RMSE values for InSAR and SPAMS, relative to the extensometer, are approximately 5.5 mm and 5.8 mm, respectively. The RMSE between InSAR and SPAMS is around 4.7 mm. The $\hat{\sigma}^2$-statistic is roughly 0.9, indicating model adequacy.

An additional validation is performed using an extensometer installed on one of the parcels inside the area of interest, marked by the star point in Figure 1. This extensometer is used as reference data to evaluate both the absolute phase estimates and the model. Figure 3 plots the extensometer data together with InSAR-based relative elevation estimates and the SPAMS model. The evaluation metrics described using RMSE and $\hat{\sigma}^2$ test statistic. The InSAR and SPAMS estimates yield RMSE values of approximately 5.5 mm and 5.8 mm, respectively, when compared to extensometer data. The calculated $\hat{\sigma}^2$ test statistic of roughly 0.9 suggests the modeled elevation changes are statistically adequate.

4 Data Records

The SPAMS10 dataset over the Krimpenerwaard region in the Netherlands is available through the 4TU.ResearchData repository: doi.org (Lumban-Gaol et al., 2025). The main data file, stored in a parquet format, contains a set of 10 SPAMS parameters per evaluated parcel. It includes the coordinates of its center-of-mass and relevant contextual information for each parcel. The

https://doi.org/10.5194/essd-2026-143
Preprint. Discussion started: 9 March 2026

contextual information includes the identifier of the closest meteorological station and the soil code describing the shallow soil type. The meteorological station identifiers in this dataset is according to the Royal Netherlands Meteorological Institute KNMI. Details about soil code can be found in the PDOK-BRO repository. A companion JSON file provides detailed schema definitions, including parameter units and interrelationships, to facilitate automated data integration and interpretation. The dataset is distributed under a Creative Commons Attribution 4.0 International (CC BY 4.0) license.

5 Usage Notes

The SPAMS10 dataset is intended for a range of applications, including subsidence forecasting under climate change scenarios, assessment of groundwater management interventions, and gap-filling in InSAR time series analysis. The dataset is compatible with open-source geospatial analysis tools and can be readily imported into Python-based workflows using the pyspams library. Example code and integration guides are provided in the dataset documentation to support reproducible research and practical implementation.

6 Code and data availability

The SPAMS10 dataset over the Krimpenerwaard region in the Netherlands is available through the 4TU.ResearchData repository: https://doi.org/10.4121/dfbe9109-d058-4a64-a5b4-1cc9d9a5f836 (Lumban-Gaol et al., 2025). The dataset is distributed under a Creative Commons Attribution 4.0 International (CC BY 4.0) license.

The computations presented in this work were done with InSAR software package, DECADE, developed by the Geodesy team at Delft University of Technology. A Python implementation to create a realization of relative surface elevation using a set of estimated SPAMS10, along with utilities for loading and analyzing the SPAMS10 dataset, is available at https://github.com/TUDelftGeodesy/pyspams.

Author contributions. Y.L. and R.F. are the main contributors. Y.L. contributed to the original draft, visualization, and data curation. R.F. contributed to editing and reviewing.

Competing interests. The authors declare that they have no known competing financial interests or personal relationships that could have appeared to influence the work reported in this paper.

Acknowledgements. This research is supported by the Indonesian Endowment Fund for Education (LPDP)

https://doi.org/10.5194/essd-2026-143
Preprint. Discussion started: 9 March 2026

Open Access Earth System Science Data Discussions

References

Ansari, H., De Zan, F., and Bamler, R.: Efficient Phase Estimation for Interferogram Stacks, IEEE Transactions on Geoscience and Remote Sensing, 56, https://doi.org/10.1109/TGRS.2018.2826045, 2018.

Arikan, M., Van Leijen, F., Guang, L., and Hanssen, R.: Improved image alignment under the influence of elevation, in: European Space Agency, (Special Publication) ESA SP, 649 SP, ISSN 03796566, 2008.

Burbey, T. J.: Extensometer forensics: what can the data really tell us?, Hydrogeology Journal, 28, 637–655, https://doi.org/10.1007/s10040-019-02060-6, 2020.

Conroy, P. and Hanssen, R.: An upper bound on carbon emissions of drained peat soils from satellite radar interferometry, ESS Open Archive, https://doi.org/10.22541/essoar.174188327.73827739/v1, 2025.

Conroy, P., van Diepen, S. A., and Hanssen, R. F.: SPAMS: A new empirical model for soft soil surface displacement based on meteorological input data, Geoderma, 440, 116 699, 2023.

Conroy, P., Lumban-Gaol, Y., Van Diepen, S., Van Leijen, F., and Hanssen, R. F.: First Wide-Area Dutch Peatland Subsidence Estimates Based on InSAR, in: IGARSS 2024-2024 IEEE International Geoscience and Remote Sensing Symposium, pp. 10 732–10 735, IEEE, 2024.

Evans, C. D., Callaghan, N., Jaya, A., Grinham, A., Sjogersten, S., Page, S. E., Harrison, M. E., Kusin, K., Kho, L. K., Ledger, M., Evers, S., Mitchell, Z., Williamson, J., Radbourne, A. D., and Jovani-Sancho, A. J.: A Novel Low-Cost, High-Resolution Camera System for Measuring Peat Subsidence and Water Table Dynamics, Frontiers in Environmental Science, 9, https://doi.org/10.3389/fenvs.2021.630752, 2021.

Ferretti, A., Prati, C., and Rocca, F.: Permanent Scatterers in SAR Interferometry, IEEE Trans Geosci Remote Sens, 39, 8–20, https://doi.org/10.1109/TGRS.2011.2124465, 2001.

Galloway, D. L. and Burbey, T. J.: Review: Regional land subsidence accompanying groundwater extraction, Hydrogeology Journal, 19, https://doi.org/10.1007/s10040-011-0775-5, 2011.

Gambolati, G., Putti, M., Teatini, P., Camporese, M., Ferraris, S., Stori, G. G., Nicoletti, V., Silvestri, S., Rizzetto, F., and Tosi, L.: Peat land oxidation enhances subsidence in the Venice watershed, Eos, Transactions American Geophysical Union, 86, 217–220, https://doi.org/10.1029/2005EO230001, 2005.

Gambolati, G., Putti, M., Teatini, P., and Gasparetto Stori, G.: Subsidence due to peat oxidation and impact on drainage infrastructures in a farmland catchment south of the Venice Lagoon, Environmental Geology, 49, 814–820, https://doi.org/10.1007/s00254-006-0176-6, 2006.

Hanssen, R. F.: Radar Interferometry: Data Interpretation and Error Analysis (Remote Sensing and Digital Image Processing), Kluwer Academic Publishers, Dordrecht, ISBN 978-0-7923-6945-5, https://doi.org/10.1007/0-306-47633-9, 2001.

Hoogland, T., van den Akker, J., and Brus, D.: Modeling the subsidence of peat soils in the Dutch coastal area, Geoderma, 171-172, 92–97, https://doi.org/10.1016/j.geoderma.2011.02.013, 2012.

Hooijer, A., Page, S., Jauhiainen, J., Lee, W. A., Lu, X. X., Idris, A., and Anshari, G.: Subsidence and carbon loss in drained tropical peatlands, Biogeosciences, 9, 1053–1071, https://doi.org/10.5194/bg-9-1053-2012, 2012.

Kampes, B. and Usai, S.: Doris: the Delft Object-oriented Radar Interferometric Software, in: 2nd International Symposium on Operationalization of Remote Sensing, vol. 1620, ISSN 0029-5582, 1999.

Kampes, B. M., Hanssen, R. F., and Perski, Z.: Radar interferometry with public domain tools, in: European Space Agency, (Special Publication) ESA SP, 550, ISSN 03796566, 2004.

https://doi.org/10.5194/essd-2026-143
Preprint. Discussion started: 9 March 2026

Krige, D. G.: A statistical approach to some mine valuation and allied problems on the Witwatersrand, Master's thesis, University of Witwatersrand, 1951.

Lumban-Gaol, Y., Conroy, P., and Hanssen, R.: SPAMS10 Krimpenerwaard: Soil motion parameters to model relative surface elevation changes, https://doi.org/10.4121/dfbe9109-d058-4a64-a5b4-1cc9d9a5f836, 2025.

Page, S., Morrison, R., Malins, C., Hooijer, A., Rieley, J., and Jaujiainen, J.: Review of peat surface greenhouse gas emissions from oil palm plantations in Southeast Asia, Tech. rep., 2011.

Pleijter, M. and van den Akker, J.: Onderwaterdrains in het veenweidegebied : toelichting op de methode en meetinrichting, no. 1586 in Alterra-rapport, Alterra, Netherlands, 2007.

Schothorst, C.: Subsidence of low moor peat soils in the western Netherlands, Geoderma, 17, 265–291, https://doi.org/10.1016/0016-7061(77)90089-1, 1977.

Stephens, J. C., Allen, L. H., and Chen, E.: Organic soil subsidence, in: Man-Induced Land Subsidence, vol. 6, pp. 107–122, Geological Society of America, https://doi.org/10.1130/REG6-p107, 1984.

Teunissen, P.: Testing Theory; an introduction, TU Delft OPEN Publishing, Delft, 3 edn., ISBN 978-94-6366-892-7, https://pure.tudelft.nl/ws/portalfiles/portal/214132690/Testing_Theory.pdf, 2024.

van Asselen, S., Stouthamer, E., and van Asch, T.: Effects of peat compaction on delta evolution: A review on processes, responses, measuring and modeling, Earth-Science Reviews, 92, 35–51, https://doi.org/10.1016/j.earscirev.2008.11.001, 2009.

van Asselen, S., Erkens, G., Stouthamer, E., Woolderink, H. A., Geeraert, R. E., and Hefting, M. M.: The relative contribution of peat compaction and oxidation to subsidence in built-up areas in the Rhine-Meuse delta, The Netherlands, Science of The Total Environment, 636, 177–191, https://doi.org/10.1016/j.scitotenv.2018.04.141, 2018.

Van Asselen, S., Erkens, G., and De Graaf, F.: Monitoring shallow subsidence in cultivated peatlands, in: Proceedings of the International Association of Hydrological Sciences, vol. 382, ISSN 2199899X, https://doi.org/10.5194/piahs-382-189-2020, 2020.

van Huissteden, J., van den Bos, R., and Marticorena Alvarez, I.: Modelling the effect of water-table management on CO 2 and CH 4 fluxes from peat soils, Netherlands Journal of Geosciences - Geologie en Mijnbouw, 85, 3–18, https://doi.org/10.1017/S0016774600021399, 2006.

Van Leijen, F.: Persistent Scatterer Interferometry based on geodetic estimation theory, Ph.D. thesis, Delft University of Technology, 2014.

Wösten, J. H., Ismail, A. B., and Van Wijk, A. L.: Peat subsidence and its practical implications: A case study in Malaysia, Geoderma, 78, https://doi.org/10.1016/S0016-7061(97)00013-X, 1997.

Zanello, F., Teatini, P., Putti, M., and Gambolati, G.: Long term peatland subsidence: Experimental study and modeling scenarios in the Venice coastland, Journal of Geophysical Research: Earth Surface, 116, https://doi.org/10.1029/2011JF002010, 2011.